Meteoritics & Planetary Science 39, Nr 12, 2033–2041 (2004)
Abstract available online at http://meteoritics.org

Ion microprobe U-Th-Pb dating and REE analyses of phosphates in the nakhlites Lafayette and Yamato-000593/000749

Kentaro TERADA[1, 2*] and Yuji SANO[3]

[1]Department of Earth and Planetary System Sciences, Hiroshima University, Higashi-Hiroshima 739–8526, Japan
[2]Project Center of Multi-Isotope Research for Astro- and Geochemical Evolution (MIRAGE), Hiroshima University, Higashi-Hiroshima 739–8526, Japan
[3]Center for Advanced Marine Research, Ocean Research Institute, The University of Tokyo, Nakanoku, Tokyo 164–8639, Japan
*Corresponding author. E-mail: terada@sci.hiroshima-u.ac.jp

(Received 9 December 2002; revision accepted 18 October 2004)

Abstract–U, Th, and Pb isotopes and rare earth elements (REEs) in individual phosphate grains from martian meteorites Lafayette and Yamato-000593/000749 were measured using a sensitive high-resolution ion microprobe (SHRIMP). Observed U-Pb data of 12 apatite grains from Yamato (Y-) 000593/000749 are well represented by linear regressions in both "conventional" 2D isochron plots and the 3D U-Pb plot (total Pb/U isochron), indicating that the formation age of this meteorite is 1.53 ± 0.46 Ga (2σ). On the other hand, the data of nine apatite grains from Lafayette are well represented by planar regression rather than linear regression, indicating that its formation age is 1.15 ± 0.34 Ga (2σ) and that a secondary alteration process slightly disturbed its U-Pb systematics as discussed in the literature regarding Nakhla. The observed REE abundance patterns of the apatites in Lafayette and Yamato-000749, normalized to CI chondrites, are characterized by a progressive depletion of heavy REEs (HREEs), a negative Eu anomaly, similarity to each other, and consistency with previously reported data for Nakhla. Considering the extensive data from other radiometric systems such as Sm-Nd, Rb-Sr, Ar-Ar, and trace elements, our results suggest that the parent magmas of the nakhlites, including the newly found Y-000593/000749, are similar and that their crystallization ages are ~1.3 Ga.

INTRODUCTION

Studies of the SNC meteorites (Shergotty, Nakhla, Chassigny) thought to be impact ejecta from the planet Mars have contributed significantly to the understanding of the planet's igneous history. Nakhlites, which are fine-grained clinopyroxenites (e.g., McSween 1994), were not subjected to severe shock metamorphism like shergottites, and their original igneous textures are well preserved. For a long time, only three nakhlites (Nakhla, Governador Valadares, and Lafayette) had been identified (Burragato et al. 1975; Berkley et al. 1980). Recently, new nakhlites, Northwest Africa (NWA) 817 and 998, and Yamato (Y)-000593/000749, were found in the Sahara desert by meteorite hunters (Sautter et al. 2002) and in Antarctica by the 41st Japanese Antarctic Research Expedition (Imae et al. 2002), respectively. Including these new findings, the nakhlite group is still considered "rare" among the SNC meteorites (currently ~30).

So far, an enormous amount of work on the radiometric dating of nakhlites (mainly Nakhla, Lafayette, and Governador Valadares) has been reported. For Nakhla, Podosek (1973) reported an $^{40}Ar/^{39}Ar$ age of ~1.3 Ga, and Papanastassiou and Wasserburg (1974) and Gale et al. (1975) used the Rb-Sr systematics to determine ages of 1.31–1.37 Ga and 1.24 ± 0.01 Ga, respectively. For Lafayette, Podosek (1973) and Podosek and Huneke (1973) originally determined an age of 1.33 ± 0.03 Ga by the $^{40}Ar/^{39}Ar$ plateau technique. Shih et al. (1998) determined a Rb-Sr age of 1.26 ± 0.07 Ga and a Sm-Nd age of 1.32 ± 0.05 Ga for the same meteorite. Governador Valadares' age has been determined by Bogard and Husain (1977) through $^{40}Ar/^{39}Ar$ dating to be 1.32 ± 0.04 Ga, while Wooden et al. (1979) reported a Rb-Sr age of 1.33 ± 0.01 Ga and Shih et al. (1999) reported a Sm-Nd age of 1.37 ± 0.02 Ga and a Rb-Sr age of 1.20 ± 0.05 Ga. Thus, the results of all these radiometric dating techniques clearly indicate a formation age of ~1.3 Ga for nakhlites. U-Pb work has only been performed for Nakhla; however, the interpretations of the U-Pb isotopic system are debatable (Hutchison et al. 1975; Chen and Wasserburg 1986a; Nakamura et al 1982; Jagoutz and Jotter 2000; Jagoutz et al. 2001). Generally, Pb-Pb isochron plots of leach-residue fractions show considerable scatter indicating that ^{207}Pb-^{206}Pb ages are >2 Ga. Nakamura

et al. (1982) reported a U-Pb concordia plot after common lead correction and subtraction of contaminant of Pb, showing the data intersecting the concordia curve at 4.33 ± 0.08 Ga and 1.28 ± 0.05 Ga (see Fig. 4 in Nakamura et al. 1982). Considering the REE measurement and Rb-Sr age of 1.26 Ga, and assuming appropriate common lead correction, Nakamura et al. (1982) concluded that the age of the light REE (LREE)-depleted Nakhla source is <4.33 Ga. Thus, a U-Pb age of 1.3 Ga for nakhlites has not yet been reported, and consensus has not been reached concerning the U-Pb systematics in nakhlites.

Recently, Jagoutz et al. (2002) contributed to the understanding of the U-Pb systematics of Nakhla. To define the initial Pb isotopic composition of Nakhla, they crushed and successfully separated plagioclase and pyroxene grains into Fe-rich rims and low-Fe cores, and measured the Pb isotopic compositions in each fraction. Their data suggested that while the plagioclase and core of the pyroxene retain the isotopic signature of the original crystallizing magma, the Pb isotopic compositions of some Fe-rich rims may have been altered by a later penetrating fluid derived from an isotopically different source.

To further understand the U-Pb systematics of nakhlites, the inner areas of individual phosphate grains from Lafayette and Y-000593/000749, which are the main host phases of U, were investigated using the sensitive high-resolution ion microprobe (SHRIMP) installed at Hiroshima University, Japan. To reduce the model dependency on common lead composition, we used the 3D U-Pb plot (total Pb/U isochron method), which has been successfully applied to the martian meteorites Shergotty (Sano et al. 2000) and Allan Hills (ALH) 84001 (Terada et al. 2003), the lunar meteorite Elephant Moraine (EET) 96008 (Anand et al. 2003), and ordinary chondrites (Terada and Sano 2002, 2003). Taking advantage of the high spatial resolution (~10 μm in this study) and the high sensitivity at high-mass resolution of SHRIMP, the REE concentrations on the same analytical spots were also measured.

SAMPLE DESCRIPTION AND ANALYTICAL METHODS

A polished thin section of Lafayette (USNM 1505-2) was provided by The National Museum of Natural History, Smithsonian Institution, and polished thin sections of Y-000593 (No. 63-1) and Y-000749 (No. 5-4) were provided by the National Institute of Polar Research in Japan. The samples were carbon-coated, and backscattered electron images were taken. Major element chemical compositions were determined by an electron probe micro analyzer (EPMA;

Table 1. Major element compositions of calcium phosphate in the Lafayette meteorite.

Meteorite	Mineral	Grain size[a] (μm × μm)	CaO (%)	MgO (%)	FeO (%)	Na_2O (%)	P_2O_5 (%)	Total (%)
Lafayette-01	Apatite	10 × 30	51.7	0.1	0.7	0.1	38.8	91.4
Lafayette-02	Apatite	15 × 25	53.4	0.1	0.8	0.1	39.7	94.1
Lafayette-03	Apatite	20 × 20	52.9	<0.1	0.7	0.1	38.7	92.4
Lafayette-04	Apatite	20 × 60	52.3	0.1	0.8	0.1	39.1	92.4
Lafayette-05	Apatite	15 × 25	51.7	0.1	0.6	0.1	38.1	90.7
Lafayette-06	Apatite	10 × 10	52.4	0.1	1.0	<0.1	38.8	92.3
Lafayette-07	Apatite	10 × 50	52.2	<0.1	0.8	<0.1	40.1	93.1
Lafayette-08	Apatite	10 × 70	53.5	0.1	1.0	0.1	39.4	94.0
Lafayette-09	Apatite	30 × 30	52.8	0.1	0.7	0.1	40.0	93.6
Lafayette-10	Apatite	10 × 10	53.3	0.1	0.9	0.1	39.8	94.2
Y-000593-1.1	Apatite	7 × 60	50.1	0.2	1.4	0.1	38.3	90.1
Y-000593-2.2	Apatite	50 × 50	53.3	<0.1	0.7	<0.1	40.8	94.9
Y-000593-3.3	Apatite	20 × 140	53.2	0.1	1.1	<0.1	40.3	94.7
Y-000593-3.4	Apatite	20 × 60	54.3	0.1	0.8	<0.1	41.0	96.2
Y-000593-4.5	Apatite	20 × 40	54.0	0.1	0.8	<0.1	41.1	95.9
Y-000593-4.6	Apatite	20 × 20	53.1	<0.1	0.8	<0.1	41.1	95.1
Y-000593-5.7	Apatite	30 × 40	53.7	0.1	1.1	<0.1	40.9	95.7
Y-000593-5.8	Apatite	40 × 160	53.5	<0.1	0.9	<0.1	41.1	95.6
Y-000749-1.1	Apatite	15 × 50	53.7	0.1	1.0	<0.1	40.5	95.4
Y-000749-2.2	Apatite	20 × 30	53.3	<0.1	0.7	<0.1	40.3	94.4
Y-000749-3.3	Apatite	15 × 50	53.0	<0.1	0.6	<0.1	41.5	95.2
Y-000749-4.4	Apatite	30 × 40	53.6	0.2	0.9	<0.1	40.9	95.6
Y-000749-5.5	Apatite	20 × 40	54.3	0.1	1.3	<0.1	40.5	96.2
Y-000749-5.6	Apatite	30 × 30	54.3	<0.1	0.8	<0.1	40.8	95.9
Y-000749-5.7	Apatite	20 × 80	52.9	0.2	1.7	<0.1	39.7	94.5
Y-000749-6.8	Apatite	20 × 60	50.5	0.2	3.3	<0.1	39.0	93.0

[a]Minor axis × major axis of individual grains.

JEOL JCMA-733II) to identify the location and mineralogy of phosphates. The sizes of the observed phosphates generally ranged 20–60 μm and the largest one has a size of 160 μm. Some of the grains have small inclusions or cracks. Table 1 lists the major element compositions of the calcium phosphates in the Lafayette meteorite. All of the observed phosphates were apatites, and were surrounded by pyroxene/augite and/or plagioclase. We did not find whitlockite, which is often observed in some shergottites and ALH 84001 (Sano et al. 2000; Terada et al. 2003). Inclusion and crack-free areas were selected for SHRIMP analysis.

After EPMA analysis, the thin sections and an epoxy resin disc with several grains of standard phosphate, "PRAP" extracted from an alkaline rock of the Prairie Lake circular complex in the Canadian Shield (Sano et al. 1999a), were introduced into SHRIMP and evacuated in the sample lock overnight to further reduce the already very small $^{x-1}PbH^+$ interference on $^{x}Pb^+$ peaks. Before the actual analysis, the ~20 μm-diameter surface of the sample was rastered for 5 min to remove the carbon coat and possible contaminants.

An ~1 nA O_2^- primary beam accelerated through a voltage of 10 kV was focused to sputter an area ~10 μm in diameter on the phosphates and positive secondary ions were extracted with 10 kV. The mass resolution was set to ~5800 at ^{208}Pb for U-Pb analyses. The magnet was cyclically peak-stepped from mass 159 ($^{40}Ca_2{}^{31}P_{16}O_3^+$) to mass 254 ($^{238}U^{16}O^+$), including background, all Pb isotopes, and masses 238 and 248 for ^{238}U and $^{232}Th^{16}O$. No significant isobaric interferences were detected in this mass range for the phosphates (e.g., the mass peak of ^{159}Tb (158.925 AMU) is clearly separated from that of $^{40}Ca_2{}^{31}P^{16}O_3^+$ (158.884 AMU) at the mass resolution of 5800). The abundance ratio of ^{238}U to ^{206}Pb was obtained from the observed $^{238}U^+/^{206}Pb^+$ ratio using an empirical quadratic relationship between the $^{206}Pb^+/^{238}U^+$ and $^{238}U^{16}O^+/^{238}U^+$ ratios of the standard apatite PRAP dated at 1156 Ma, as follows:

$$^{206}Pb/^{238}U = \frac{A \times (^{206}Pb^+/^{238}U^+)_{sample}}{(^{238}U^{16}O^+/^{238}U^+)^2_{sample}} \quad (1)$$

where A, $(^{206}Pb^+/^{238}U^+)_{sample}$, and $(^{238}U^{16}O^+/^{238}U^+)_{sample}$ denote a constant, and the observed secondary $^{206}Pb^+/^{238}U^+$ and $^{238}U^{16}O^+/^{238}U$ ratios of the sample, respectively. The constant A was obtained by repeated measurement of the standard apatite PRAP. Uranium and Th concentrations were calibrated from $^{238}U^{16}O^+/^{40}Ca_2{}^{31}P^{16}O_3^+$ and $^{232}Th^{16}O^+/^{238}U^{16}O^+$ and the U and Th contents of PRAP (196 and 172 ppm, respectively). Experimental details of the U-Pb analysis and the calibration of the data were given in Sano et al. (1999a, 2000).

The quantitative measurements of REEs in the phosphates were carried out in high-mass resolution mode. A mass resolution of 9300 at 1% peak height was employed to separate HREEs from the oxides of the LREEs in the standard phosphate PRAP with adequate flat top peaks. All isobaric interferences were mostly resolved (see Fig. 1 of Sano et al. 1999b). The magnet was cyclically peak-stepped from mass 139 ($^{139}La^+$) to mass 172 ($^{172}Yb^+$), including $^{140}Ce^+$, $^{141}Pr^+$, $^{145}Nd^+$, $^{146}Nd^+$, $^{147}Sm^+$, $^{149}Sm^+$, $^{151}Eu^+$, $^{153}Eu^+$, $^{155}Gd^+$, $^{157}Gd^+$, $^{40}Ca_2{}^{31}P^{16}O_3^+$, $^{159}Tb^+$, $^{161}Dy^+$, $^{163}Dy^+$, $^{165}Ho^+$, $^{166}Er^+$, $^{167}Er^+$, $^{169}Tm^+$, and $^{171}Yb^+$. The REE concentrations are calculated using PRAP as the reference. Details of the REE analysis and the calibration of the data were given elsewhere (Sano et al. 2002).

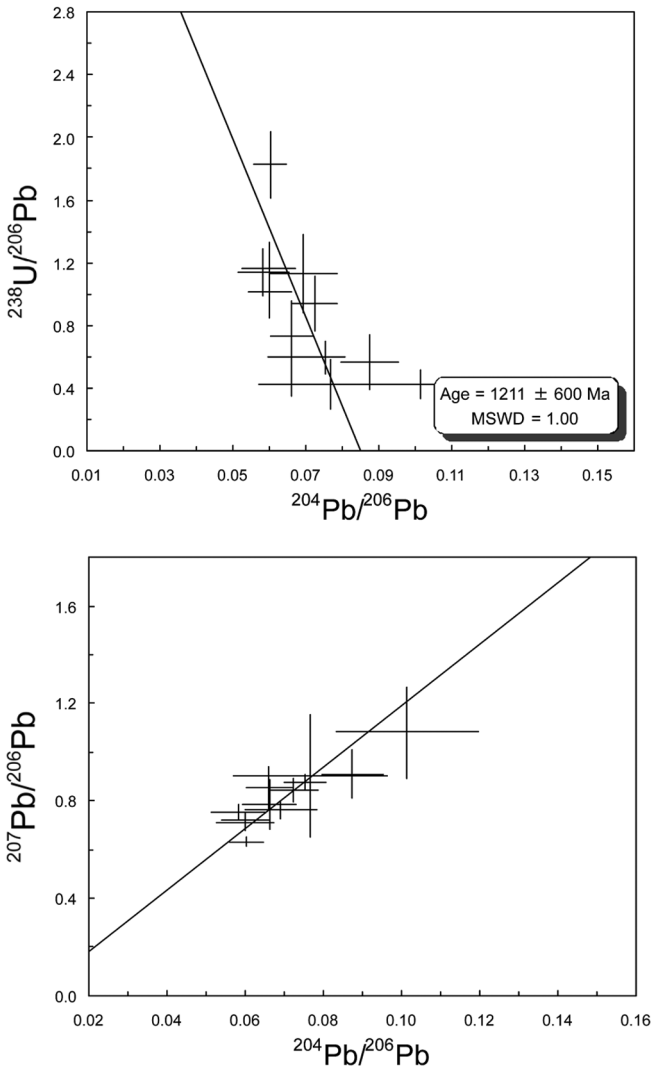

Fig. 1. Inverse U/Pb isochron diagram (top) and an inverse Pb/Pb isochron diagram (bottom) for Y-000593/000749. Errors are 1σ. Least-square fits using the York methods (York 1969) give 1211 ± 600 Ma (95% CL; MSWD = 1; error correlation = 0) for the $^{238}U/^{206}Pb$ age. A $^{207}Pb/^{206}Pb$ age could not be obtained because of large analytical uncertainties, though a correlation between $^{207}Pb/^{206}Pb$ and $^{204}Pb/^{206}Pb$ can be recognized.

RESULTS

The U and Th concentrations, $^{238}U/^{206}Pb$, $^{207}Pb/^{206}Pb$, $^{204}Pb/^{206}Pb$, $^{204}Pb/^{208}Pb$, and $^{232}Th/^{208}Pb$ ratios of each analysis are given in Table 2. Hereafter, we will treat Yamato-000593 and Yamato-000749 as a single meteorite Yamato (Y-)000593/000749 because they are considered to be paired based on mineralogical and geochemical data (Imae et al. 2002). The errors of the U and Th concentrations are ~30% at 2σ, as estimated by the repeated measurement of the standard apatite. The U and Th contents of both meteorites vary considerably, from 3 to 17 ppm, and 10–59 ppm, respectively. However, Th/U ratios range from 2.7 to 5.6 (average 4.3 ± 1.0) for Lafayette, and from 2.7 to 4.7 (average 3.6 ± 0.6) for Y-000593/000749. Although these ratios are similar for both meteorites and are comparable to that of the whole rock of Nakhla (4.36 ± 0.04 by Nakamura et al. 1982; 4.08 by Chen and Wasserburg 1986b), they are inconsistent with values previously reported by Crozaz (1979) on apatites in Lafayette using the fission track method, which indicated a U concentration in apatites of 1.5 ppm and a Th/U ratio of 10 ± 1. In addition, observed $^{238}U/^{204}Pb$ ratios, except for LAFA01.01 (not shown in Table 2), are 20~100 and consistent with that of Nakhla leaches of 25~52 by Chen and Wasserburg (1986b) and ~52 by Nakamura et al. (1982).

Table 2 shows correlations in the $^{238}U/^{206}Pb$ versus $^{204}Pb/^{206}Pb$, $^{207}Pb/^{206}Pb$ versus $^{204}Pb/^{206}Pb$, and $^{232}Th/^{208}Pb$ versus $^{204}Pb/^{208}Pb$ ratios for both meteorites. We first applied the conventional U-Pb and Pb/Pb isochron methods, then a "three-dimensional U-Pb discordia plane" in the $^{238}U/^{206}Pb$-$^{207}Pb/^{206}Pb$-$^{204}Pb/^{206}Pb$ 3D space, a method pioneered by Levchenkov and Shukolyukov (1970) (for details see Wendt 1984 and 1989). Although Ludwig (2001) referred this method as the "total Pb/U isochron," we follow Wendt (1984, 1989) and refer to the approach and the obtained age as the 3D U-Pb discordia method and the 3D U-Pb age, respectively.

U-Pb Systematics for Y-000593/000749

We first calculated the "conventional" $^{238}U/^{206}Pb$ and $^{207}Pb/^{206}Pb$ isochron ages for Y-000593/000749. Least-square fits using the York methods (York 1969) give 1211 ± 600 Ma (95% CL; MSWD = 1; error correlation = 0) for the $^{238}U/^{206}Pb$ age. A conclusive $^{207}Pb/^{206}Pb$ age could not be obtained because of large analytical uncertainties, though a correlation between $^{207}Pb/^{206}Pb$ and $^{204}Pb/^{206}Pb$ is evident (Fig. 1). Next, the regression lines in $^{238}U/^{206}Pb$-$^{207}Pb/^{206}Pb$-$^{204}Pb/^{206}Pb$ 3D space were calculated with the 3D U-Pb discordia method using Isoplot/Ex software (Ludwig 2001). At the regression lines' intersection, the $^{238}U/^{206}Pb$-$^{207}Pb/^{206}Pb$ plane falls, by definition, on the U-Pb concordia curve. The crucial advantages of this method are that knowing the isotopic composition of common Pb is unnecessary, and that the ^{238}U and ^{235}U decay schemes are simultaneously used to yield a smaller justifiable age uncertainty for the U-Pb systematics (Ludwig 2001). Twelve analyses of apatites from Y-000593/000749 indicate a 3D U-Pb age of 1.53 ± 0.46 Ga (2σ, MSWD = 0.63) with $(^{206}Pb/^{204}Pb)_{initial}$ of 10.9 ± 1.4 and $(^{207}Pb/^{204}Pb)_{initial}$ of 11.2 ± 0.8, respectively. In Fig. 2, the data

Table 2. U-Th-Pb analyses of apatites from Lafayette and Yamato-000593/000749.[a]

Spot No.	U (ppm)	Th (ppm)	Th/U	$^{238}U/^{206}Pb$	$^{207}Pb/^{206}Pb$	$^{204}Pb/^{206}Pb$	$^{204}Pb/^{208}Pb$	$^{232}Th/^{208}Pb$
LAFA01.01	37	160	4.4	0.213 ± 0.019	0.7907 ± 0.0054	0.0553 ± 0.0007	0.0259 ± 0.0004	0.444 ± 0.036
LAFA03.01	12	40	3.4	3.024 ± 0.177	0.3969 ± 0.0092	0.0279 ± 0.0013	0.0174 ± 0.0009	6.333 ± 0.344
LAFA04.01	3	19	5.6	1.147 ± 0.116	0.6561 ± 0.0141	0.0522 ± 0.0020	0.0254 ± 0.0011	3.125 ± 0.287
LAFA04.02	4	18	5.0	1.362 ± 0.137	0.6639 ± 0.0142	0.0547 ± 0.0021	0.0255 ± 0.0011	3.202 ± 0.291
LAFA04.03	5	21	4.6	1.179 ± 0.086	0.6898 ± 0.0119	0.0538 ± 0.0017	0.0262 ± 0.0009	2.663 ± 0.177
LAFA05.01	14	76	5.5	0.399 ± 0.032	0.7999 ± 0.0080	0.0644 ± 0.0012	0.0293 ± 0.0006	0.992 ± 0.071
LAFA08.01	17	59	3.5	2.671 ± 0.140	0.4505 ± 0.0068	0.0319 ± 0.0010	0.0200 ± 0.0006	5.861 ± 0.281
LAFA09.01	7	17	2.7	0.878 ± 0.083	0.7126 ± 0.0099	0.0458 ± 0.0014	0.0247 ± 0.0008	1.264 ± 0.107
LAFA10.01	8	33	4.4	0.932 ± 0.086	0.6506 ± 0.0113	0.0398 ± 0.0014	0.0214 ± 0.0008	2.200 ± 0.183
Y-000593.1	63	290	4.7	0.423 ± 0.155	0.9029 ± 0.2503	0.0768 ± 0.0196	0.0300 ± 0.0110	0.783 ± 0.332
Y-000593.2	3	10	3.1	1.013 ± 0.169	0.7225 ± 0.0290	0.0602 ± 0.0060	0.0288 ± 0.0034	1.482 ± 0.250
Y-000593.3-1	9	38	4.5	0.424 ± 0.091	1.0819 ± 0.1872	0.1015 ± 0.0182	0.0401 ± 0.0100	0.752 ± 0.199
Y-000593.3-2	4	12	3.3	0.937 ± 0.173	0.8453 ± 0.0476	0.0725 ± 0.0063	0.0308 ± 0.0032	1.326 ± 0.259
Y-000593.4	5	18	3.6	1.161 ± 0.165	0.7097 ± 0.0337	0.0599 ± 0.0074	0.0267 ± 0.0035	1.850 ± 0.266
Y-000593.5	5	12	2.7	1.828 ± 0.212	0.6311 ± 0.0187	0.0604 ± 0.0045	0.0295 ± 0.0023	2.411 ± 0.357
Y-000749.1	4	11	3.0	0.599 ± 0.250	0.7842 ± 0.1017	0.0662 ± 0.0067	0.0311 ± 0.0041	0.845 ± 0.369
Y-000749.3	25	94	3.9	0.565 ± 0.177	0.9092 ± 0.0990	0.0875 ± 0.0079	0.0361 ± 0.0053	0.917 ± 0.291
Y-000749.4	5	15	2.9	1.139 ± 0.149	0.7529 ± 0.0340	0.0583 ± 0.0070	0.0254 ± 0.0032	1.434 ± 0.190
Y-000749.5-1	5	17	3.5	0.732 ± 0.221	0.8569 ± 0.0850	0.0662 ± 0.0059	0.0294 ± 0.0050	1.137 ± 0.376

[a]The error assigned to the isotopic and elemental ratio is 1σ as estimated by counting statistics and calibration. The errors on concentration are ~±30% estimated by repeated measurements of the standard apatite PRAP. Y-000593 and Y-000749 are treated as a single meteorite because they are considered to be paired.

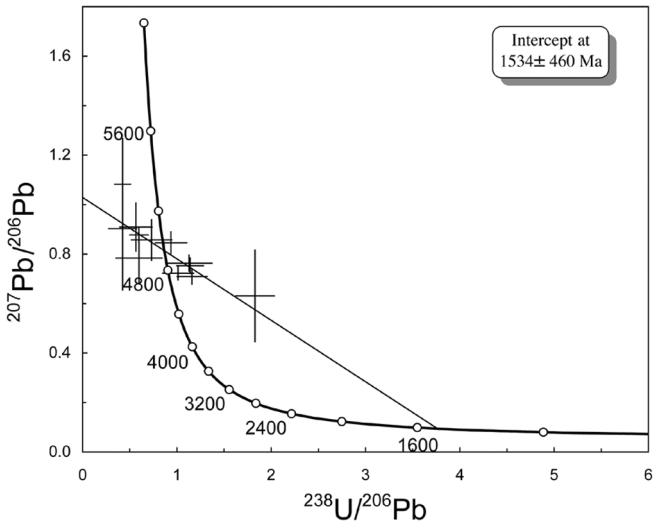

Fig. 2. The result of linear regressions of Y-000593/000749 phosphates in the $^{238}U/^{206}Pb$-$^{207}Pb/^{206}Pb$-$^{204}Pb/^{206}Pb$ space. Here, 12 apatites data and the regression line are projected onto the $^{238}U/^{206}Pb$-$^{207}Pb/^{206}Pb$ plane. Uncertainties are 1σ. The solid curve is an evolution line of the U-Pb system (concordia line). Note that the 3D U-Pb age is determined by the intersection of regression line and the concordia line on the X-Y plane, yielding 1.53 ± 0.46 Ga (2σ). The linear regressions in 3D space were obtained using Isoplot/Ex (Ludwig 2001).

and linear regression for Y-000593/000749 are shown by a plot of the $^{238}U/^{206}Pb$-$^{207}Pb/^{206}Pb$ projection using the Isoplot/Ex software (Ludwig 2001). Finally, the $^{232}Th/^{208}Pb$ ages were calculated from the correlation between the $^{232}Th/^{208}Pb$ and $^{204}Pb/^{208}Pb$ ratios in Table 2. Least-square fits using the York method (York 1969) gives 1.24 ± 2.10 Ga (2σ; MSWD = 0.51; error correlation = 0) with $(^{208}Pb/^{204}Pb)_{initial}$ = 30.4 ± 1.1 for Y-000593/000749. A conclusive age was not obtained due to the large uncertainty.

U-Pb Systematics for Lafayette

We first calculated the "conventional" $^{238}U/^{206}Pb$ and $^{207}Pb/^{206}Pb$ isochron ages for Lafayette. Least-square fits using the York methods (York 1969) give $^{238}U/^{206}Pb$ and $^{207}Pb/^{206}Pb$ isochron ages of 1301 ± 500 Ma (95% CL; MSWD = 19; error correlation = 0) and 1777 ± 3700 Ma (95% CL; MSWD = 11; error correlation = 0). The isochron plots shown in Fig. 3 show considerable scatter, causing large MSWD values. This feature is very similar to those of Nakhla as previously reported (Hutchison et al. 1975; Chen and Wasserburg 1986a).

Next, with the 3D U-Pb discordia methods, we calculated the regression lines in $^{238}U/^{206}Pb$-$^{207}Pb/^{206}Pb$-$^{204}Pb/^{206}Pb$ 3D space. Nine analyses of apatites from Lafayette indicate a 3D U-Pb age of 1.12 ± 0.27 Ga (2σ, MSWD = 9.8) with $(^{206}Pb/^{204}Pb)_{initial}$ of 16.4 ± 1.1 and $(^{207}Pb/^{204}Pb)_{initial}$ of 13.7 ± 0.9. Since the MSWD value was large, a 3D U-Pb age obtained for

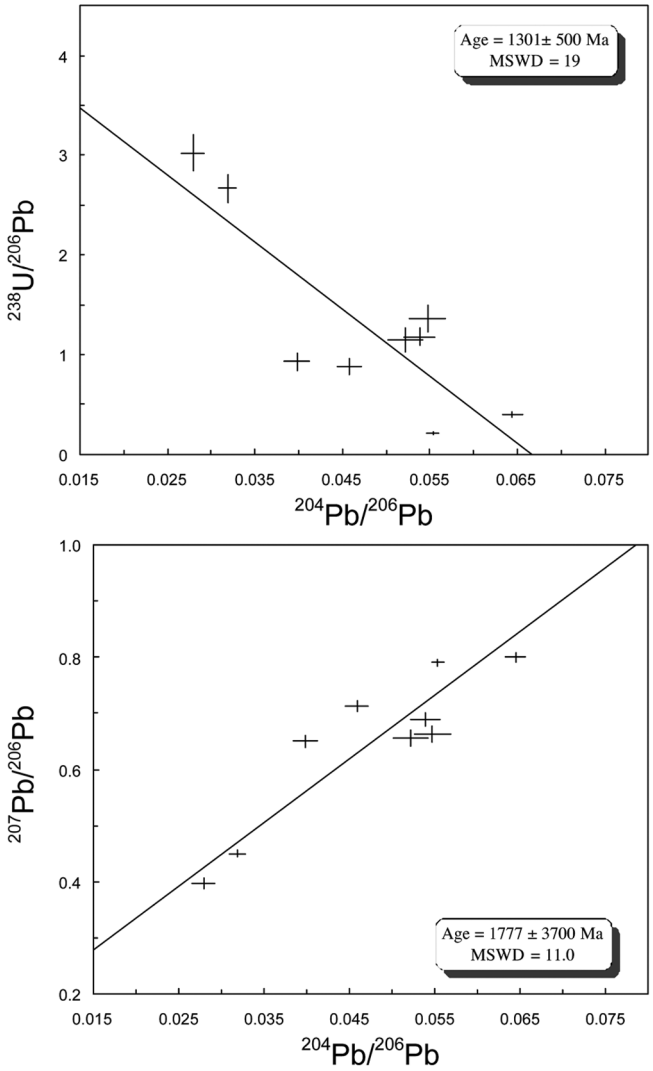

Fig. 3. An inverse U/Pb isochron diagram (top) and an inverse Pb/Pb isochron diagram (bottom) for Lafayette. Errors are 1σ. Least-square fits using the York methods (York 1969) give $^{238}U/^{206}Pb$ and $^{207}Pb/^{206}Pb$ isochron ages of 1301 ± 500 Ma (95% CL; MSWD = 19; error correlation = 0) and 1777 ± 3700 Ma (95% CL; MSWD = 11; error correlation = 0). These isochron plots show considerable scatter, causing large MSWD values. This feature is very similar to those of Nakhla as previously reported (Hutchison et al. 1975; Chen and Wasserburg 1986a).

Lafayette using linear regression may not be appropriate. Therefore, we finally adopted the planar regression in 3D space. The 3D least-square fit using the Isoplot/Ex software shows that the nine observed data sets can be fitted to a plane Y = aX + b + cZ (that is, $[^{207}Pb/^{206}Pb] = a[^{238}U/^{206}Pb] + b + c[^{204}Pb/^{206}Pb]$), with a = –0.110 ± 0.018, b = 0.642 ± 0.087, and c = 3.1 ± 1.4 (2σ; MSWD = 0.88). It should be noted that the initial Pb composition of Y-000593/000749 ($[^{206}Pb/^{204}Pb]_{initial}$ = 10.9 ± 1.4 and $[^{207}Pb/^{204}Pb]_{initial}$ = 11.2 ± 0.8) plot on the intersection line of the Lafayette plane with the Y-Z plane (that is, Y = b + cZ). Figure 4 shows the data

Table 3. Rare earth element concentrations (ppm) in phosphate from Lafayette and Y-000749.[a]

Element	Y749.01	Y749.03	Y749.06	LAFA.01	LAFA.02	LAFA.03	LAFA.04	LAFA.05	LAFA.06
La	419.4	547.7	244.3	680.5	943.9	466.3	516.6	706.1	487.1
Ce	1210.4	1707.1	678.2	1547.0	2232.9	1132.7	1278.5	1609.3	1229.0
Pr	166.1	207.2	106.4	206.2	317.1	158.9	179.2	222.4	184.1
Nd	688.4	1040.9	467.6	707.6	1249.2	589.3	559.2	761.4	682.7
Sm	131.1	145.7	95.4	126.5	209.6	97.9	81.8	113.8	123.9
Eu	26.0	34.9	21.9	20.9	19.1	9.1	12.0	13.5	11.0
Gd	99.8	141.4	95.7	101.8	167.3	62.3	55.8	79.3	85.6
Tb	17.9	24.2	14.2	16.9	22.8	10.4	9.3	13.0	16.3
Dy	84.8	101.7	59.0	74.0	84.5	32.5	33.7	51.0	66.1
Ho	12.2	19.0	9.0	12.8	14.2	6.4	5.8	8.3	12.0
Er	34.3	45.1	23.2	28.8	32.7	12.6	11.8	17.4	23.7
Tm	4.1	5.7	2.7	3.1	3.5	1.8	1.5	2.2	3.2
Yb	24.3	28.8	12.5	15.5	12.3	6.5	8.0	11.6	17.1
Sum REE[b]	2918.7	4049.4	1830.1	3541.7	5308.9	2586.6	2753.1	3609.3	2941.8
Eu/Eu[c]	0.67	0.73	0.69	0.54	0.30	0.33	0.51	0.41	0.31
Yb/La	0.09	0.08	0.08	0.03	0.02	0.02	0.02	0.02	0.05

[a]The relative errors of the measurements are ±30% as estimated from the reproducibility of the standard sample.
[b]The sum of the REE does not include the Lu content because of large uncertainty.
[c]Eu/Eu is Eu × 2/(Sm + Gd), where the concentrations are normalized to CI chondrite.

projected parallel to the $^{204}Pb/^{206}Pb$ axis (filled circles), and parallel to the regression plane (the common Pb subtracted data; open diamonds), and the intersect line of the best-fit plane with the $^{238}U/^{206}Pb$-$^{207}Pb/^{206}Pb$ plane. This planar regression provides the upper and lower concordia intercept age of 4.32 ± 0.32 Ga and 1.15 ± 0.34 Ga (2σ), respectively. These features will be discussed in the next section.

The $^{232}Th/^{208}Pb$ age was also calculated based on the correlation between the $^{232}Th/^{208}Pb$ and $^{204}Pb/^{208}Pb$ ratios given in Table 2. Least-square fits using the York method (York 1969) gives 1.38 ± 0.69 Ga (2σ; MSWD = 9.5; error correlation = 0) with $(^{208}Pb/^{204}Pb)_{initial}$ = 33.3 ± 7.8. The large MSWD of Lafayette could be caused by the complicated U-Th-Pb systematics (discussed below), as well as those of linear regression in the 3D U-Pb method used for Lafayette.

Rare Earth Element Analyses

Rare earth element concentrations of the phosphates in Lafayette and Y-000749 are given in Table 3. Figure 5 shows REE abundance patterns normalized to CI chondrites. Most apatites show a progressive depletion of the HREEs (i.e., Yb/La ratios range between 0.02– 0.09) accompanied by negative Eu anomalies (i.e., Eu/Eu^* ~0.3–0.7, where Eu^* is arithmetically calculated from (Sm + Gd)/2, the concentrations of which are normalized to CI chondrite values). Except for the Eu anomaly, these features of the REE patterns are very similar to those previously reported by Wadhwa and Crozaz (1995). Generally, the negative Eu anomalies of Y-000749 (Eu/Eu^* ~0.7) are smaller than those of Lafayette, (Eu/Eu^* ~0.3–0.5, present study), and Nakhla (Wadhwa and Crozaz 1995). For comparison, their data are also shown in Fig. 5.

DISCUSSION

The REE abundances of the constitutive minerals augite, olivine, plagioclase, and apatites in Nakhla and Lafayette have been well documented by Wadhwa and Crozaz (1992, 1995). They reported that apatite contains the highest REE abundances in both Nakhla and Lafayette and that the REE patterns of each mineral are very similar to each other. Moreover, based on mass balance calculations, Wadhwa and Crozaz (1992) suggested that apatite makes up ~0.5% of the minerals in both Nakhla and Lafayette and that it accounts for ~85% of the La, ~30% of the Eu, and ~50% of the HREE present in the whole rocks. With the exception of ~20% of the Eu in the plagioclase, which shows a positive Eu anomaly (Eu/Eu^* ~20–30), most of the remaining REE are located in augite. If this is the case, good agreement with the REE pattern of Y-000749 and those of Lafayette and previous analyses, suggests that a similar mass balance (i.e., similar distributions of REE among different minerals) might have occurred in Y-000749 meteorites. The slight differences in the degree of the Eu negative anomaly among these nakhlites could be interpreted as differences in the abundance of plagioclase around the phosphate grains in the local area of ~100 μm scale.

The U-Pb data of 12 apatite grains from Y-000593/000749 are well represented by linear regressions in both "conventional" 2D isochron plots and the 3D U-Pb plot (total Pb/U isochron plot), indicating a formation age of 1.53 ± 0.46 Ga (2σ). The U-Pb data of the nine apatite grains from Lafayette are well represented by a planar regression rather than linear regressions, indicating concordia intercept ages of 4.32 ± 0.32 Ga and 1.15 ± 0.34 Ga (2σ), respectively. This feature of U-Pb systematics of Lafayette is very similar to those of Nakhla, where the data correlation line intersects the concordia curve at 4.33 ± 0.08 Ga and 1.28 ± 0.05 Ga after

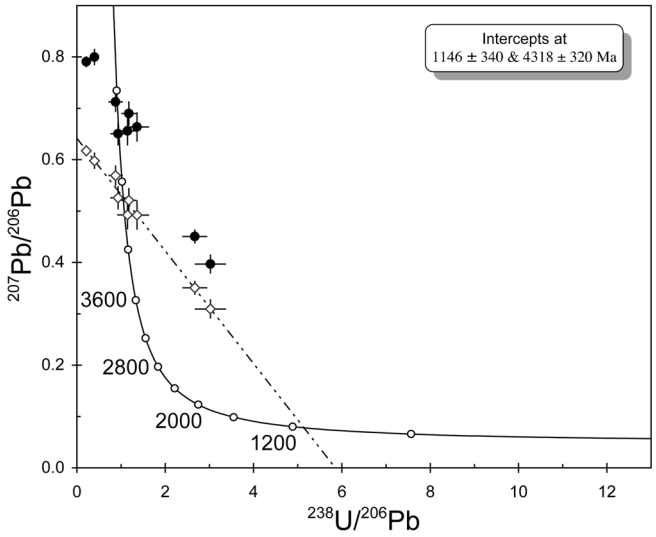

Fig. 4. The result of planar regressions of Lafayette phosphates in the $^{238}U/^{206}Pb$-$^{207}Pb/^{206}Pb$-$^{204}Pb/^{206}Pb$ space. Raw data (filled circles) are corrected for the presence of initial Pb by a 3D projection from the $^{238}U/^{206}Pb$-$^{207}Pb/^{206}Pb$-$^{204}Pb/^{206}Pb$ space parallel to the best-fit planar regression of the raw data. The corrected data are shown by a black cross. Uncertainties are 1σ. The solid curve is an evolution line of the U-Pb system (concordia line), and the dot-dashed line for the corrected data intersects the concordia curve at 1.15 ± 0.34 Ga and 4.32 ± 0.32 Ga (2σ). Taking into account other radiogenic ages, the older age is apparently an arithmetical solution but not a geological age (see the text). The planar regression in 3D space was obtained using Isoplot/Ex (Ludwig 2001).

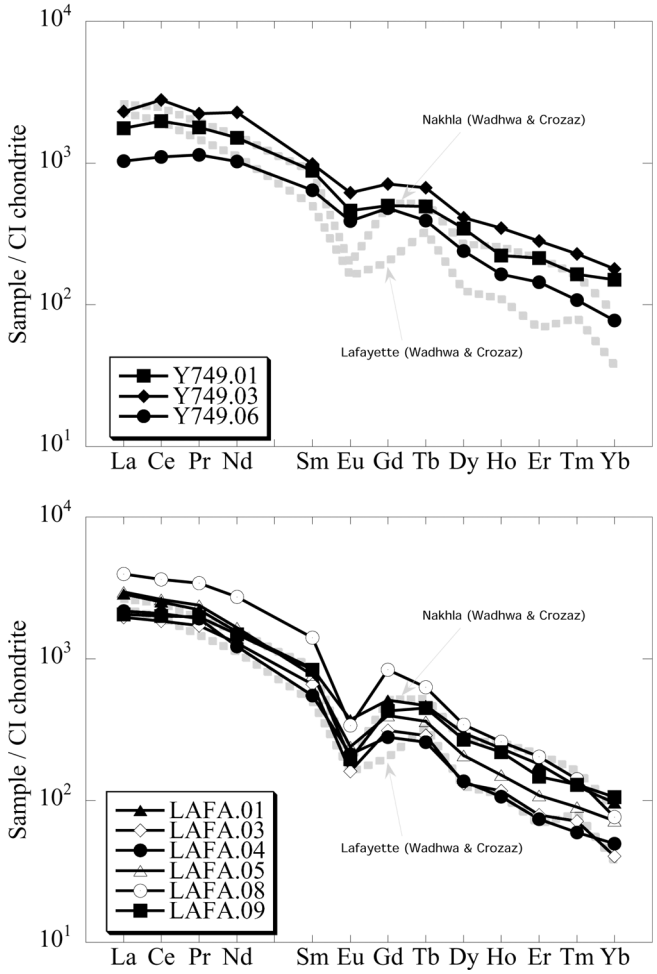

Fig. 5. CI normalized (from Anders and Grevesse 1989) REE abundance patterns of phosphates from Yamato-000749 and Lafayette (solid lines). For comparison, those of Lafayette and Nakhla reported by Wadhwa and Crozaz (1995) are shown as gray broken lines.

corrections for both Canyon Diablo troilite Pb and terrestrial Pb contamination are made (Nakamura et al. 1982). Chen and Wasserburg (1986b) similarly obtained two intercepts with the concordia curve at 4.26 ± 0.04 Ga and 1.13 ± 0.10 Ga by investigating an interior piece of Nakhla. Here, it is noted that our results do not assume the isotopic composition of common lead.

In general, the planar regression of U-Pb discordia data in the $^{238}U/^{206}Pb$-$^{207}Pb/^{206}Pb$-$^{204}Pb/^{206}Pb$ 3D space can be interpreted by two kinds of geological case (for example, see Ludwig 2001). One is the combination of a linear discordia on the X-Y plane and one point of common Pb component on the Y-Z plane (case I). In this case, both upper and lower intercept ages are geologically valid, corresponding to a formation age and an alteration age, respectively. Another case is the combination of the one concordant age on the X-Y plane and a mixing line on the Y-Z plane (case II). In case II, the upper intercept age is an artifact, not a geological age. Here, it should be noted that the younger age is geochronologically valid in both case I and II. Taking into account the extensive data obtained from other radiometric systems (Rb-Sr age of 1.27 ± 0.07 Ga, Sm-Nd age of 1.32 ± 0.05 Ga by Shih et al. [1998] and Ar/Ar plateau age of 1.33 ± 0.03 Ga by Podosek [1973] and Podosek and Huneke [1973]), we conclude that our age for Y-000593/000749 (1.53 ± 0.46 Ga) and younger age of Lafayette (1.15 ± 0.34 Ga) define the crystallization age of apatites in Nakhlite, and that the planar distribution of data points in the 3D space for Lafayette can be explained by a secondary alteration process as previously discussed for Nakhla (Jagoutz et al. 2002).

Figure 6 illustrates this complicated U-Pb systematics for Lafayette, Y-000593/000749, and Nakhla. It is noted that this diagram is a projection onto the Y-Z plane of $^{238}U/^{206}Pb$-$^{207}Pb/^{206}Pb$-$^{204}Pb/^{206}Pb$ 3D space. The data of Lafayette and Y-000593/000749 are plotted as a red circle and blue squares, respectively. For comparison, those of Nakhla (Nakamura et al. 1982) are also shown as green circles. The blue line is an isochron line determined from the initial lead composition of Y-000593/000749 (“A”) and the radiogenic Pb isotopic ratio of 1.3 Ga (“C”), which is the projected regression line on the Y-Z plane of Y-000593/000749. The yellow area is the intersection (with uncertainties) between the planar regression for Lafayette and the Y-Z plane, corresponding to a mixing array in case II. Lead growth curves with various